

The Three-Dimensionality of Spiral Shocks: Did Chondrules Catch a Breaking Wave?

A. C. Boley and R. H. Durisen

*Indiana University, Astronomy Department, 727 E. Third St., Bloomington, IN
47405-7105, USA*

M. K. Pickett

*Purdue University Calumet, Department of Chemistry and Physics, 2200 169th
St., Hammond, IN 46323-2095, USA*

Abstract. Spiral shocks in vertically stratified disks lead to hydraulic/shock-jumps (hs-jumps) that stimulate large scale (tenths of an AU or more) radial and vertical motions, breaking surface waves, high-altitude shocks, and vortical flows. These effects are demonstrated by three-dimensional hydrodynamics simulations in Solar Nebula models. Trajectories of fluid elements, along with their thermal histories, suggest that hs-jumps mix the nebular gas and provide diverse pre-shock conditions, some of which are conducive to chondrule formation. In addition, hs-jumps may provide an energy source for driving nebular turbulence to size-sort chondrules.

1. Introduction

Shocks within the Solar Nebula are a favored mechanism for thermally processing chondritic material. One-dimensional shock calculations with radiative physics have shown that melting chondrule precursors via frictional gas drag heating, followed by immersion in the slowly cooling post-shock gas, produces the requisite high cooling rates above the liquidus and more moderate cooling rates during crystallization (Iida et al. 2001; Desch & Connolly 2002; Ciesla & Hood 2002; also see Desch et al., this volume). A shock mechanism also seems favorable because it forms chondrules in the disk. Fine-grained rims suggest a disk origin due to the positive correlation between rim thickness and chondrule diameter (Morfill et al. 1998). Additionally, the matrix-chondrule abundances indicate that chondrules and the matrix material formed from the same reservoir of gas (Palme et al. 1993). Even though shocks have been shown to be capable of reproducing chondrule thermal histories, there is not a widely accepted mechanism for producing chondrule-forming shocks. Boss & Durisen (this volume) critique the various proposed mechanisms and conclude that spiral waves (Wood 1996) are the most promising.

Spiral waves in disks are often described as density waves. However, this is not strictly correct in a vertically stratified disk with an equation of state (EOS) that is stiffer than an isothermal gas. Under realistic nebular conditions these waves behave more like f -modes than density waves (Pickett et al. 1998, 2000; Ogilvie 2002; Durisen et al. 2003). As a spiral wave passes through a protoplanetary disk, the post-shock region is overpressured, and it will expand in the vertical direction (Boley et al. 2005, in preparation). In simulations of the Galaxy, Martos & Cox (1998) noted that, when the

otherwise isothermal gas is stiffened by a magnetic field, spiral shocks have characteristics of hydraulic jumps. A classical hydraulic jump occurs in an incompressible fluid, where the only way to reduce the kinetic energy of fluid elements coming into the wave is to convert it to gravitational potential or turbulent energy (Massey 1970). Examples of hydraulic jumps can be found in spillways when there is an abrupt change in slope and the slowly moving water has a greater height than the rapidly moving water. As we will show, spiral waves in vertically stratified disks have a hydraulic jump-like morphology. We will therefore refer to these waves as hydraulic/shock-jumps (hs-jumps) to emphasize their hybrid nature.

Hs-jumps drive surface waves that break and dissipate near the disk surface and that transport fluid elements vertically and radially. High-altitude shocks are created where the wave breaks, and these must be considered when investigating the thermal histories of fluid elements in disks. These waves underscore the importance of the shock's three-dimensionality. It is the purpose of this paper to demonstrate the morphology of hs-jumps and then determine pre-shock conditions in several simple Solar Nebula models with driven spiral shocks. Furthermore, we will briefly discuss how hs-jumps might provide a mechanism for generating turbulence in the disk and driving chondrule size-sorting.

2. Numerical Hydrodynamics

2.1. Hydrodynamics Code

Our simulations are calculated using the Indiana University Hydrodynamics Group (IUHG) code (see Pickett et al. 1998, 2000, 2003; Mejía 2004; Mejía et al. 2005). It solves for the hydrodynamics equations of motion, with self-gravity, on an Eulerian cylindrical grid (r, φ, z) and is second-order in space and time. Outflow boundaries are used at the inner, outer, and upper grid boundaries, and reflection symmetry is assumed about the equatorial plane. The self-gravity component of the potential is calculated directly from the Poisson equation and a multipole expansion of spherical harmonics is used for the boundaries with $\ell, m \leq 10$ (Pickett 1995). The code runs in parallel on the Indiana University-Purdue University Indianapolis IBM SP supercluster.

2.2. Initial Models

Three initial equilibrium disks are evolved, which we call light, moderate, and massive, based on the mass they contain within 6 AU of the Sun. These disks are subjected to different types of perturbations, which drive spiral waves into the chondrite producing region. Although, as in Boss & Durisen (this volume), we believe that gravitational instabilities at or beyond 5 AU will be responsible for producing the shock-triggering perturbations, we do not attempt to build fully self-consistent models. The initial disks are gravitationally stable and are only evolved for a few rotations at 5 AU. The disk equilibrium models are generated for the IUHG code using a self-consistent field (SCF) method (Hachisu 1986; Pickett et al. 1996). Due to the nature of the SCF method, the EOS is restricted to be a barotrope, so we assume our initial disk is polytropic where $P = K\rho^\gamma$ for K constant everywhere and γ is the ratio of specific heats. The star is then cut out of the model, and its mass and potential are saved and treated appropriately as a point mass. Since this changes the equilibrium configuration, the model is then

evolved axisymmetrically, without heating or cooling, in a 2D version of the IUHG code until the disk has adjusted to the new, slightly different potential.

We model the 1 to 6 AU region for each disk around a $1 M_{\odot}$ star. The gas is assumed to be monatomic and ideal, so $\gamma = 5/3$. The light disk was generated to contain $0.0130 M_{\odot}$ within 6 AU. The surface density has a profile $\Sigma(r) \propto r^{-0.5}$, which yields a $\Sigma(5.2\text{AU}) = 830 \text{ g/cm}^2$. Assuming that the surface density profile breaks to $\Sigma(r) \propto r^{-1.5}$ beyond 6 AU (cf. Lissauer 1987; Boss 2002) the total mass contained within 40 AU is $0.0747 M_{\odot}$. The temperature profile out to 6 AU falls as r^{-1} . The light disk has a Toomre Q of about 10 near 5.2 AU and is greater than 10 for smaller radii. The Toomre (1964) $Q = c_s \kappa / \pi G \Sigma$, where c_s is the sound speed and κ is the epicyclic frequency, is a parameter that indicates whether a disk is gravitationally stable. If $Q < 1.5$, gravitational instabilities will set in (Durisen et al. 2003).

The moderate disk was generated to contain $0.0370 M_{\odot}$ inside 6 AU. Assuming a similar surface density profile as the light disk, it contains $0.213 M_{\odot}$ inside 40 AU and has a surface density at 5.2 AU of $\Sigma(5.2 \text{ AU}) = 2360 \text{ g/cm}^2$. The Q value is 5 near 5.2 AU.

Table 1. Parameters for the different disk models. The indicated disk mass is for inside 6 AU. The most promising altitude (MPA) column highlights the altitude in the disk where chondrule formation is most promising. The Q column indicates the Toomre Q value at 5.2 AU. The last column, R, indicates the grid resolution (r, φ, z) , where $1 \rightarrow (256, 128, 64)$, $2 \rightarrow (256, 512, 64)$, and $3 \rightarrow (256, 512, 32)$. Where two resolutions are used, the higher resolution does not change the general trend of pre-shock conditions that fluid elements encounter. We intend to investigate all future disks at high resolution.

$M_d (r < 6 \text{ AU})$ (M_{\odot})	Perturber	r_{pert} (AU)	$\Sigma(5.2 \text{ AU})$ (g cm^{-2})	MPA	Q(5.2 AU)	R
1.30(-2)	0.5 M_J	5.2	830	Midplane	10	1
1.30(-2)	5.0 M_J	5.2	830	Midplane	10	1,2
3.70(-2)	5.0 M_J	5.2	2360	Midplane	5	1,2
3.70(-2)	10.0 M_J	4.8	2360	Moderate	5	1
1.43(-1)	$\cos(2\phi)$	4.8	9130	High	2	3

The massive disk is a variant of the Pickett et al. (2003) High- Q disk but with the initial outer radius scaled to 6 AU. Such scaling places $0.143 M_{\odot}$ within 6 AU. Assuming the same surface density profile as the light disk, the total disk mass within 40 AU is $0.822 M_{\odot}$ and the surface density at 5.2 AU is $\Sigma(5.2\text{AU}) = 9130 \text{ g/cm}^2$. The Q value for this disk is near 2 at 5 AU so it is only marginally stable there. We realize that this disk is much more massive than the minimum-mass Solar Nebula, usually cited to be between $0.01\text{-}0.1 M_{\odot}$ (Weidenschilling 1977). It was the first disk model we ourselves used to study the properties of hs-jumps, but it could correspond either to an extremely early phase of Solar Nebula evolution or to a phase when mass had built up between 1 and 10 AU in a dead zone (Gammie 1996; Armitage et al. 2001).

2.3. Shocks

Two methods are used for producing shocks. The first method, applied only to the massive disk, places a $\cos(2\phi)$ corotating potential perturbation at 4.8 AU with a FWHM in radius of about 0.48 AU. The perturbation maximum is 5% of the total potential at that radius. This forces two spiral arms to form, and we refer to this as the forced-shock run. The second method introduces a point mass near 5 AU on a circular, Keplerian orbit. Perturbations with masses of $0.5 M_J$ and $5.0 M_J$ are used for the light disk and $5.0 M_J$ and $10.0 M_J$ for the moderate disk. The point masses produce spiral wakes (Ogilvie & Lubow 2002), so we refer to these simulations as the wake-shock runs. There is a large volume of parameter space that we have yet to investigate, and our purpose here is only to present several preliminary test cases. Midplane density greyscales are shown in Figure 1 for the forced-shock run and for one wake-shock run.

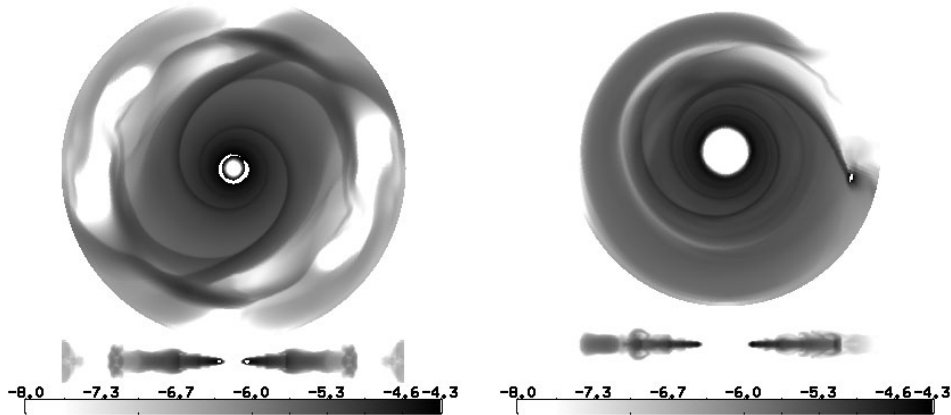


Figure 1. Midplane and r - z logarithmic density greyscales for the forced-shock run (left) and the light disk $5 M_J$ wake-shock run (right). The units for the greyscale are given in code units. The conversion to real units is $3.54(-4)$ and $4.47(-5)$ g/cc per code unit respectively. The other wake-shock runs have similar morphologies to the one shown here. Note the breaking waves in the r - z cross-sections.

Spiral shocks are intrinsically three-dimensional, and a two-dimensional interpretation of spiral waves in vertically stratified disks conceals their true nature. Consider the pre-shock gas to be in vertical hydrostatic equilibrium. As the pre-shock gas enters the shock, the gas is compressed, changing the vertical self-gravity and the vertical gas pressure. Define the parameter $q \equiv (\partial\Phi_*/\partial z) / (\partial\Phi_{g_1}/\partial z)$, which represents the relative importance of the central potential Φ_* to the pre-shock gas self-gravity Φ_{g_1} . As self-gravity becomes negligible, $q \rightarrow \infty$. By using the Rankine-Hugoniot shock conditions for an adiabatic gas, we define the jump-factor

$$J_f \equiv \left(\frac{1}{\rho_2} \frac{\partial P_2}{\partial z} \right) \left(\frac{1}{\rho_1} \frac{\partial P_1}{\partial z} \right)^{-1} \left(\frac{\partial \Phi_1}{\partial z} \right) \left(\frac{\partial \Phi_2}{\partial z} \right)^{-1} \quad (1)$$

$$= \frac{2\gamma\mathcal{M}^4(\gamma-1) - \mathcal{M}^2(1-6\gamma+\gamma^2) - 2(\gamma-1)}{\mathcal{M}^2(\gamma+1)^2} \left[\frac{q+1}{q + \frac{\mathcal{M}^2(\gamma+1)}{2+\mathcal{M}^2(\gamma-1)}} \right], \quad (2)$$

where $\mathcal{M} = \sqrt{u^2 \rho_1 / \gamma P_1}$ is the Mach number of the shock, u is the gas velocity in the frame of the shock, P_1 and ρ_1 are the pre-shock gas pressure and density, P_2 and ρ_2 are the post-shock pressure and density, and Φ_1 and Φ_2 are the total pre- and post-shock potentials (see Boley et al. 2005, in preparation for more detail). If we assume that $q \gg 1$ and recall that the pre-shock gas is in vertical hydrostatic equilibrium, the vertical acceleration behind the shock is

$$a_z = - \left(\frac{1}{\rho_2} \frac{\partial P_2}{\partial z} + \frac{\partial \Phi_2}{\partial z} \right) \quad (3)$$

$$= - \frac{\partial \Phi_2}{\partial z} \left[J_f \frac{1}{\rho_1} \frac{\partial P_1}{\partial z} \left(\frac{\partial \Phi_1}{\partial z} \right)^{-1} + 1 \right] \approx \Omega_r^2 z (J_f - 1), \quad (4)$$

where Ω_r is the circular angular speed at r . What can be seen from (4) is that the gas will expand in the vertical direction for $J_f > 1$ and collapse when $J_f < 1$. For most protoplanetary disk conditions J_f will be greater than unity, typically around four for these calculations, and the gas will expand. We refer to this expansion as an h-jump, and the consequences are shown by the velocity field in Figure 2 and by the fluid element trajectories in Figure 3. Nebular material at high z is forced in the vertical direction, and some material is transported radially over large Δr in surface waves. Radial motions develop because the motion perpendicular to the shock is slowed as the gas passes through the shock, while the tangential component is unaffected. The net result is that the gas jumps and moves inward. In Figure 2, one can see a tall, vertical shock front tracing the inner edge of the spiral that extends from the midplane to moderate disk altitudes. However, there are additional shocks at moderate to high disk altitudes that result when the surface wave crashes back onto the disk. The volumetric heating rates for these high-altitude shocks are just as great as for the vertical shock. Note the large vortical flow created by the wave centered near $z = 0.3$ AU and $r = 2.35$ AU.

Model parameters and shock types are indicated in Table 1. Although our chosen parameters suggest that one should interpret our shocks as perturbations caused by a proto-Jupiter, such an interpretation is misleading. An object with a mass greater than $0.1 M_J$ will clear a gap after several orbits (Bate et al. 2003) and suppress the strength of the spiral shocks. If a planet were growing via core-accretion, a gap would be cleared before the resulting spiral would become strong enough to produce chondrules. Instead, we consider the point masses to be massive transient gas clumps (see Fig. 6 in Boss and Durisen, this volume). These clumps could be the result of gravitational instabilities in a surface density enhanced ring (Durisen et al. 2005) or dead zone (Gammie 1996; Desch 2004).

3. Fluid Element Histories

Velocity field data stored from the hydrodynamics simulations are used to integrate fluid element trajectories by a fourth-order Runge-Kutta integration scheme, while the associated density and internal energy data are used to infer thermal histories. Since the data are large, the temporal resolution is limited, and data are stored, approximately, every 1/100-1/50 pattern period. Quantities are linearly interpolated between two data sets for every time step.

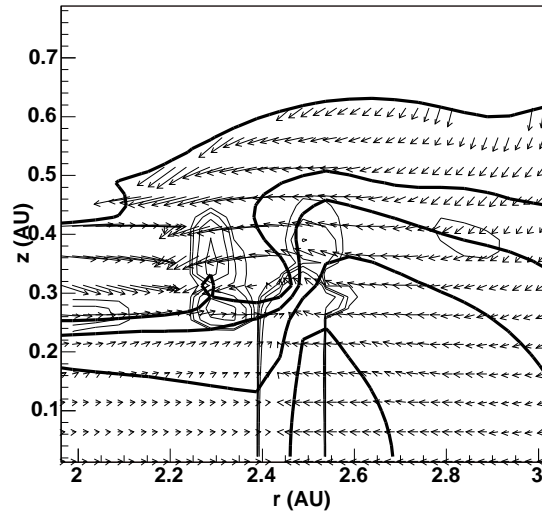


Figure 2. Radial slice of the forced-shock run. The arrows represent relative gas velocities scaled to each axis appropriately. The thick solid contours are density contours of $2.81(-12)$, $3.54(-10)$, $7.08(-10)$, $1.42(-9)$, $2.83(-9)$ g/cc. The thin solid contours represent volumetric heating rates produced by shocks: $3.51(-8)$, $7.02(-8)$, $1.40(-7)$, $2.81(-7)$ erg/s/cc. The spiral wave leads to a hs-jump, which includes the tall vertical shock front and the gas flowing up and over it. The resulting surface wave crashes back onto the disk creating high-altitude shocks and vortical flows. The forced-shock run is the cleanest case to examine since it has two, well-defined spiral arms. The wake-shock runs have multiple arms with varying midplane densities creating many hs-jumps. The shock and vertical morphologies for these runs are very complex. An animation of the breaking wave in this figure is available at <http://westworld.astro.indiana.edu/>.

The global 3D nature of the problem limits the resolution of the hydrodynamics code. The shocks themselves are not well-resolved. The typical cell size in our calculations is approximately 4×10^{11} cm while the width of radiative-shock peaks seen in 1D calculations are only of the order of 10^8 cm and the entire heating and cooling range is about 10^{10} cm. So the peak densities and temperatures of shocks in the IUHG code represent conditions far behind the shock in 1D calculations. The purpose of this work is to identify where spiral shocks provide environments that are conducive to chondrule formation. Our fluid element trajectories can detect when particles pass through shocks, and will accurately determine pre-shock conditions. We can then compare these pre-shock parameters with the detailed 1D shock simulations (e.g., Desch & Connolly 2002) to determine whether these shocks would create chondrule producing conditions.

The $10.0 M_J$ moderate-disk run provides a broad range of thermal histories and very complex fluid element trajectories. As shown in Figure 3, the shocks lead to complicated vertical and radial motions. The fluid elements moving through the perturbed disk experience multifarious shock conditions. For example, the thermal history of the fluid element in Figure 3 for the moderate- z trajectory shows many temperature spikes

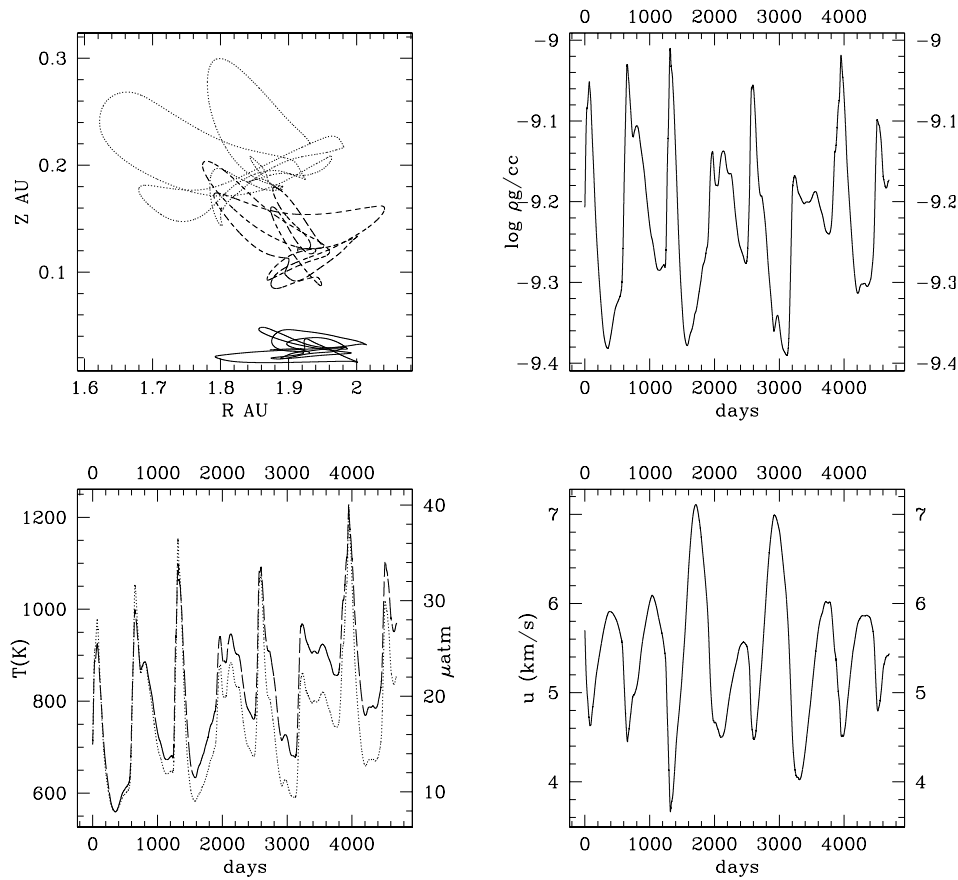


Figure 3. The moderate disk and $10 M_J$ perturber. *Top-left*: Trajectories for fluid elements at three different initial disk altitudes. Notice the complex radial and vertical motions. *Top-right*: The density history of the middle-altitude fluid element's trajectory. Each spike corresponds to a shock. The actual peak of each spike cannot be resolved with the 3D code (see text). Note the range of pre-shock densities associated with the trajectory. *Bottom-left*: Temperature (solid) and pressure (dotted) history of the middle-altitude fluid element. As for the density, the peaks are not necessarily representative of the shock strengths. *Bottom-right*: Velocity normal to the shock in the frame of the shock (see text). Using u and pre-shock conditions from the other plots, one may characterize shock strengths. Although the pre-shock conditions are not exactly what are required by Desch & Connolly (2002) they are close to them and diverse. Additionally, if one of the above shocks forms chondrules, the solids are likely to have a different history than the fluid element from that shock forward.

between 1000 and 1200 K, but our simulations capture only the broad post-shock region. The narrow 1D chondrule-producing regions of shocks are not resolved. Each peak corresponds to a different pre-shock temperature, pressure and density. To calculate the gas velocity normal to the shock in the frame of the shock, u , we make the assumption that the spiral shocks have approximately the same pitch angle i for all r . With this assumption one can measure the pitch angle, near 20° for our runs, and

calculate u by

$$u = v_r \cos i + (\Omega_r - \Omega_{\text{pattern}}) r \sin i. \quad (5)$$

For shocks that have a significant vertical component, e.g., shocks resulting from breaking waves, this method is not accurate. However, it does give a decent measure for a large number of shocks in the disk. As shown in Figure 3, the u for many of the shocks is around 5-5.5 km/s. Although the densities and relative shock velocities are not ideal for chondrule formation, they indicate that a large range of conditions is possible. A statistical approach examining many fluid element trajectories will be required to address whether such a disk forms chondrules in the asteroid belt region.

Fluid elements in the forced-shock run also have complex thermal histories and trajectories. However, only at high-disk altitudes do the pre-shock conditions fall within the favorable range defined by Desch & Connolly (2002). At moderate and low disk altitudes, the disk may be too hot. At radii greater than approximately 2.5 AU, where temperatures and pressures are more favorable in the midplane, the relative shock velocities are too low. However, if a perturber further out than 5 AU created a spiral wake, hs-jumps could be capable of forming chondrules at low to mid-disk altitudes for the massive case.

The 0.5 M_J and the 5 M_J light-disk runs yield different results. The thermal histories¹ show many heating events. None yield the required peak temperatures and pressures in the 3D hydro simulations. However, this is due to the code's inability to resolve the shocks, as explained above. If we look at the pre-shock conditions, the story is more favorable. Fluid elements, near the midplane, at about 1.5 AU encounter the shock at speeds of 7 km/s with gas densities of about 10^{-9} g/cc in the midplane. Pre-shock temperatures are well below 650 K, typically around 350 K, with a pressure around 8×10^{-6} atm. These conditions fall in the chondrule producing range according to Desch & Connolly (2002). At higher disk altitudes and larger radii, the densities are no longer conducive to chondrule formation. For the inner radii the relative shock speeds become too large and the pre-shock temperatures may become too large as well. The 5 M_J moderate-disk run shows results similar to the light disk.

4. Discussion

A challenge to any chondrule formation theory is to explain not only heating and cooling rates, but also the present location of chondritic material, the wide variety of chondrules seen, how chondrules were produced for several million years, and how they were size-sorted. For the runs discussed here, chondrule-forming pre-shock conditions occur between 1.5 and 2.5 AU for perturbations originating around 5 AU. This chondrule-producing "sweet-spot" is set by the density, temperature distribution, and the nature of the perturbation, all of which are likely to change with time. If clump formation is transient and episodic, then several clumps may exist at the same time. This would create more complex shock structures than what are presented here and might shift the chondrule-forming region. If clump formation is repetitious, clumps may form at different radii to produce spatially changing chondrule-forming regions. As the disk evolves, the locale of the shocks change so that different chondrule types

¹More thermal histories as well as disk and shock animations are viewable at <http://westworld.astro.indiana.edu/>.

may form at specific radii in the disk and be subsequently scattered once collected into their parent bodies. Additionally, as the disk loses mass, the formation location also changes, because the pre-shock conditions are greatly altered. Transient clump formation throughout the disk's lifetime could drive hs-jumps and provide a wide range of pre-shock conditions over several million years.

The fluid element trajectories also indicate that nebular material is moved radially and vertically. The vertical motions are consistent with what is expected from an hs-jump, i.e., the material at higher disk altitudes is expected to show more aggressive vertical motions. Associated with these vertical motions are radial excursions of the fluid elements from their initial radii. In accordance with the f -mode character at the spiral waves, the radial excursions are larger for material at high-disk altitude. Therefore one might expect to have stronger shocks above the midplane, inasmuch as the radial velocity component is more normal to these moderate pitch angle spirals than the azimuthal component. The midplane may not be the only favorable environment for chondrule formation and the nebular material may remain mixed throughout its lifetime.

The breaking waves could additionally provide a source of turbulence needed to size-sort the newly processed chondrule material (Cuzzi et al. 2001). Notice, for instance, the large scale vortical motion associated with the breaking wave in Figure 2. We can test whether it is feasible for hs-jumps to provide enough turbulence for size-sorting. Consider

$$k = \alpha_k c_s^2 / 2, \quad (6)$$

where α_k is the viscous scaling parameter based on k , the turbulent kinetic energy per gram. If we assume that k is some fraction f of the energy E_j that powers an hs-jump, we can get an order of magnitude estimate of α_k . Assume that we can use the vertical velocity V_z of a high-altitude jumping fluid element to estimate E_j by $V_z^2/2$, and rewrite (6) as

$$\alpha_k = f \frac{V_z^2}{c_s^2} = f \frac{3V_z^2 \rho}{5P}. \quad (7)$$

If we assume that $\alpha_k \approx \alpha_\nu$, the shear viscosity parameter, then the necessary α_k for size-sorting is approximately between 10^{-3} and 10^{-4} (Cuzzi et al. 2001). To get $\alpha_k \sim 10^{-3}$ requires only $f \approx 0.02$, using the peak values of the shock at 1200 days in Figure 3 wherein the fluid element has a post-shock vertical velocity of about 0.5 km/s.

We argue that global spiral shocks provide a way to mix nebular material, form chondrules, and drive chondrule size-sorting turbulence over several million years. In this scenario, chondrule precursors would experience a multitude of pre-shock conditions based on their physical and temporal formation location. We believe that our results, although still somewhat crude, suggest that global spiral shocks formed the chondritic material seen today.

Acknowledgments. We thank K. Cai, S. Desch, A. Nelson, and an anonymous referee for their help in preparing this manuscript. We especially thank S. Michael for his contributions to this manuscript. This work was supported in part by Shared University Research grants from IBM, Inc. to Indiana University. A. C. B. and R. H. D. were supported by NASA Origins of Solar Systems grant No. NAG5-11964.

References

Armitage, P. J., Livio, M., & Pringle, J. E. 2001, MNRAS, 324, 705

- Bate, M. R., Lubow, S. H., Ogilvie, G. I., & Miller, K. A. 2003, *MNRAS*, 341, 213
Boss, A. P. 2002, *ApJ*, 576, 462
Ciesla, F. J. & Hood, L. L. 2002, *Icarus*, 158, 281
Cuzzi, J. N., Hogan, R. C., Paque, J. M., & Dobrovolskis, A. R. 2001, *ApJ*, 546, 496
Desch, S. J. 2004, *ApJ*, 608, 509
Desch, S. J. & Connolly, H. C. 2002, *Meteorit. & Planet. Sci.*, 37, 183
Durisen, R. H., Cai, K., Mejía, A. C., & Pickett, M. K. 2005, *Icarus*, in press
Durisen, R. H., Mejía, A. C., & Pickett, B. K. 2003, *Recent Research Development in Applied Physics*, 1, 173
Gammie, C. F. 1996, *ApJ*, 457, 355
Hachisu, I. 1986, *ApJs*, 62, 461
Iida, A., Nakamoto, T., Susa, H., & Nakagawa, Y. 2001, *Icarus*, 153, 430
Lissauer, J. J. 1987, *Icarus*, 69, 249
Martos, M. A. & Cox, D. P. 1998, *ApJ*, 509, 703
Massey, B. S. 1970, *Mechanics of Fluids*, 2nd Edition (Van Norstrand Reinhold Company)
Mejía, A. C. 2004, Ph.D. thesis, Indiana University
Mejía, A. C., Durisen, R. H., Pickett, M. K., & Cai, K. 2005, *ApJ*, in press
Morfill, G. E., Durisen, R. H., & Turner, G. W. 1998, *Icarus*, 134, 180
Ogilvie, G. I. 2002, *MNRAS*, 330, 937
Ogilvie, G. I. & Lubow, S. H. 2002, *MNRAS*, 330, 950
Palme, H., Spettel, B., & Ikeda, Y. 1993, *Meteoritics*, 28, 417
Pickett, B. K. 1995, Ph.D. Thesis
Pickett, B. K., Cassen, P., Durisen, R. H., & Link, R. 1998, *ApJ*, 504, 468
Pickett, B. K., Cassen, P., Durisen, R. H., & Link, R. 2000, *ApJ*, 529, 1034
Pickett, B. K., Durisen, R. H., & Davis, G. A. 1996, *ApJ*, 458, 714
Pickett, B. K., Mejía, A. C., Durisen, R. H., Cassen, P. M., Berry, D. K., & Link, R. P. 2003, *ApJ*, 590, 1060
Toomre, A. 1964, *ApJ*, 139, 1217
Weidenschilling, S. J. 1977, *ApSS*, 51, 153
Wood, J. A. 1996, *Meteorit. & Planet. Sci.*, 31, 641